ARTICLE

Ionic Space-Charge Effects in Solid State Organic Photovoltaics

Martijn Lenes and Henk J. Bolink*

Instituto de Ciencia Molecular, Universidad de Valencia, PO Box 22085, Valencia, Spain

ABSTRACT The effect of mobile ions on the operation of donor−acceptor bilayer solar cells is studied. We demonstrate the large effect ions can have on the energetics of the solar cells, illustrated by (for instance) changing the output voltage of a cell in situ from 0.35 to 0.74 V. More importantly, it is shown ionic species do not obstruct the charge generating properties of the photovoltaic devices and ionic space charge can be used in situ to improve their efficiencies. The results obtained are explained by taking into account energetic changes at the donor−acceptor interface as well as built-in potentials, giving clear guidelines on how ionic species can offer many new and exciting functionalities to organic photovoltaics.

KEYWORDS: organic photovoltaics • ionic-electronic conductivity • cyanine dyes

INTRODUCTION

In organic electronics, the ability to support both ionic and electronic conduction is regarded as one of the possibilities to go beyond traditional device architectures and achieve exciting and new functionalities (1, 2). Examples in which such mixed systems are employed include electrochromic devices, artificial muscles, biosensors, and thin film light-emitting devices. In the latter, the incorporation of mobile ions was first done in 1995 yielding luminescent devices, with strongly reduced turn-on voltages and allowing the use of air-stable electrodes (3). In these devices referred to as light emitting electrochemical cells (LECs), typically, there is one layer of a mixed ionic electronic conductor sandwiched in between two electrodes. Upon application of an electric field, the mobile anions (or cations, respectively) migrate to the cathode (anode) facilitating efficient charge injection. In this way, efficient electroluminescence can be achieved using a single active layer with air stable electrodes greatly simplifying the production processes (4−6). Upon the application of an external bias, the single layer is subdivided into p- and n-doped regions close to the respective electrodes separated by an undoped or intrinsic layer. Hence, it allows one to mimic the p-i-n light emitting diode by the application of an external electric field (7). Additionally, the self-organizing nature of the ions allow for interesting device geometries such as cascaded devices (8). The incorporation of ionic conductivity in light emitting devices is a relatively often pursued approach (9−11). Remarkably, in thin film photovoltaic devices, no extensive use has been made of mixed ionic and electronic conducting materials, except for dye sensitized solar cells in which ions are used as the electrochemical regeneration couple for the dyes. This is especially remarkable as the currently best performing solid state organic photovoltaic device (active area larger than 1 cm^2) utilizes the same p-i-n geometry as the light emitting devices described above (12). In analogy to the light emitting electrochemical cell, the possibility of achieving such device architectures by the movement of ions offers many advantages. For one, it would be possible to prepare such structures using solution based techniques which significantly decreases the production costs. Additionally, ionic movement can be used to tune the solar cell characteristics, which was demonstrated in a few cases, however, only in devices with very low efficiencies (13−16). Furthermore, it was proposed to use ions to assist in the charge separation process (17−19). There is, however, in general, very little knowledge concerning the effect (positive or negative) of ions on electronic and excitonic species, and a more general understanding of mixed ionically and electronically conducting systems is needed to guide future research in this field.

RESULTS AND DISCUSSION

In this article, we investigate the effect of mobile ions on the operation of bilayer solar cells based on cyanine dyes as electron donor and C_{60} as electron acceptor. The low molecular weight cyanine dyes are interesting for photovoltaic applications because of their very high absorption coefficient, solution processability, and the possibility of chemically tailoring their energy levels. In the last years, these bilayer solar cells have shown a steady increase in power conversion efficiencies reaching a maximum of 3.5% (20). For this work, the main interest in these dyes originates from their cationic nature, supplying us with the desired ionic functionality. Bilayer solar cells are made by sandwiching the cyanine dye/C_{60} heterojunction between an indium tin oxide (ITO)/poly(3,4-ethylenedioxythiophene) poly(styrenesulfonate) (PEDOT/PSS) anode and a barium/silver cathode. A layer of bathocuproine (BCP) is evaporated in between the C_{60} layer and the cathode to ensure a proper ohmic contact and, hence, an efficient charge extraction (21). Two different dyes (Cy1 and Cy2, Figure 1) are used; Cy1 has two naphthalene rings on the periphery of the

* To whom correspondence should be addressed. E-mail: henk.bolink@uv.es.
Received for review September 1, 2010 and accepted November 15, 2010

DOI: 10.1021/am1008216

Published on Web 12/01/2010

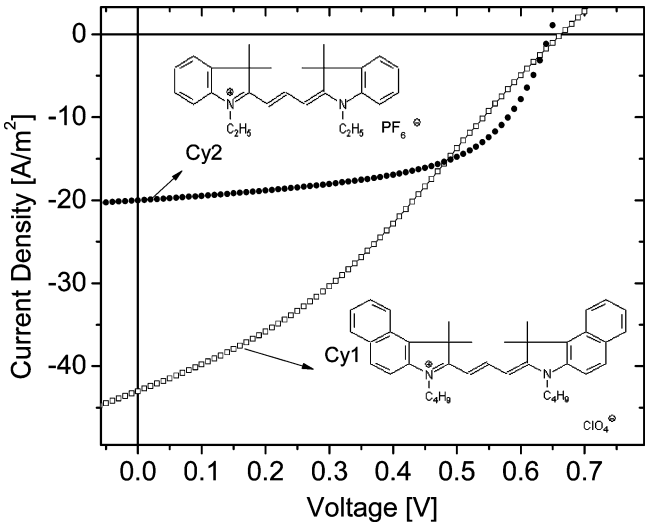

FIGURE 1. Current density to voltage characteristics of the bilayer solar cells using Cy1 (open squares) and Cy2 (filled circles) including their chemical structure.

Table 1. Solar Cell Characteristics under Illumination of 1000 W/m² Simulated Sunlight and Different Prebias Conditions[a]

device	bias conditions [V]	J_{sc} [A/m²]	fill factor [%]	V_{oc}[V]	estimated PCE [%]
Cy1/C_{60}	fresh	43.0	33.0	0.662	0.94
	+0.8	35.5	36.0	0.508	0.65
	+1.0	26.7	40.0	0.346	0.37
	−0.4	41.2	34.6	0.737	1.04
	−0.8	39.8	33.0	0.727	0.96
	−1.0	39.0	30.3	0.727	0.86
	−1.2	37.7	29.2	0.668	0.73
Cy2/C_{60}	fresh	20.0	57.2	0.645	0.74
	+0.8	19.64	56.5	0.613	0.68
	+1.0	19.2	53.5	0.606	0.62
	−0.4	20.2	53.1	0.760	0.81
	−0.8	20.5	51.7	0.794	0.84
	−1	20.4	50.8	0.811	0.84
	−1.2	20.5	49.4	0.817	0.83

[a] The order of poling follows the order in the table.

ethylene base unit whereas in Cy2, they are replaced by phenyl rings. As a result of this increased conjugation, the bandgap of Cy1 is reduced with respect to that of Cy2. The highest occupied molecular orbital (HOMO) and lowest unoccupied molecular orbital (LUMO) of the dyes are −5.4 and −3.6 eV for Cy1 and −5.5 and −3.4 eV for Cy2, as determined by cyclic voltammetry (see SI1 in the Supporting Information). Figure 1 shows the current density to voltage *(J−V)* characteristics of solar cells using the two dyes under illumination of 1000 W/m² simulated AM1.5 solar light. Reasonable efficiencies of around 1 % are obtained for both devices with the one using Cy1 showing a higher short circuit current, probably due to the smaller bandgap of the material (see IPCE spectra, SI2 in the Supporting Information). The solar cell efficiencies and characteristics (see Table 1) presented here coincide with previous values reported for similar devices (22). Devices with higher efficiencies have been obtained using similar photoactive components (a)

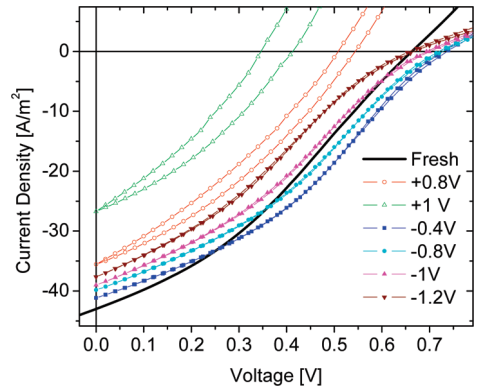

FIGURE 2. Current density to voltage characteristics of the bilayer solar cells using Cy1 under different prebias conditions. The order of poling follows the order in the legend.

when the dyes are partially oxidized (doped) or (b) by optimizing the electrode materials (20, 23).

The device employing Cy1 shows a distinct s-shape around the open circuit voltage, a feature commonly observed in cyanine dye solar cells (22, 23). This is most likely due to the relatively deep HOMO levels of the cyanine dyes compared to the workfunction of PEDOT/PSS which impedes efficient hole extraction. Recent results on similar devices employing polyaniline anodes show that this undesired behavior can be removed by the use of higher workfunction anodes (20).

In order to investigate the effect of ionic space charge on the operation of the solar cells, a constant bias was applied while illuminating the device. This bias is maintained for a few minutes until the current through the device saturates and, thus, a steady state regime is obtained (see the Supporting Information). After poling the device for several minutes, the $J-V$ characteristic is determined. To probe the effect of the $J-V$ sweep on the ionic distribution within the device, both an up and a down sweep are recorded.

Figure 2 shows the $J-V$ characteristics of the solar cell using Cy1 after poling at biases of −1.2 to +1 V. The poling and, hence, the redistribution of the ions inside the donor layer has a large effect on the operation of the solar cells. The application of a positive bias results in a strong decrease of the V_{oc}, whereas the application of a negative bias increases the V_{oc}, however, in this case, the s-shape of the curve around V_{oc} becomes more pronounced. In Table 1, all relevant solar cell characteristics before and after poling are summarized. We note that all measurements are performed on the same device and that the changes in $J-V$ curves are fully reversible (an example can be found in the Supporting Information). Furthermore, the behavior described here is observed in a large number of devices and is, hence, not device specific. In order to explain the observed behavior, we recall the origin of the open circuit voltage of bilayer solar cells. In general, the open circuit voltage of donor−acceptor solar cells is determined by the splitting of quasi-Fermi levels at the donor−acceptor interface and is, thus, primarily determined by the difference of the LUMO of the acceptor and the HOMO of the donor (24, 25). For bulk heterojunction cells, additional requirements exist to reach the theoretical

Scheme 1. Simplified Band Diagram Indicating Bending of the Donor Energy Levels after Ion Accumulation with Implications for the Maximum Open Circuit Voltage and Built-in Voltage[a]

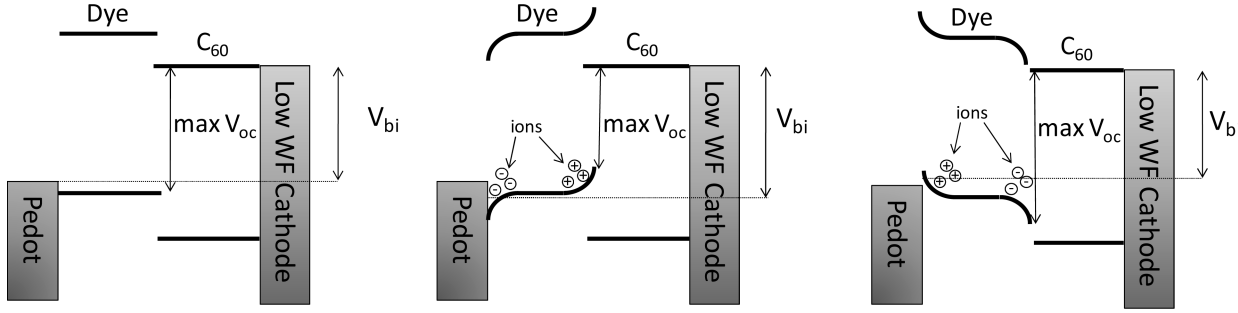

[a] Left: the fresh device; middle: the device after positive biasing; right: the device after negative biasing. The case of a Cy1/C_{60} device is depicted in which the open circuit voltage exceeds the built-in voltage.

maximum open circuit voltage. For one, the built-in voltage of the solar cell (governed by the difference in workfunction of anode and cathode) cannot be smaller than the HOMO−LUMO offset; as otherwise, this results in a reduced open circuit voltage (26). For bilayer solar cells, however, the open circuit voltage can exceed the built-in voltage of the device (27). For these devices, at voltages slightly above V_{bi}, a net photocurrent can still be sustained by the diffusion of generated charge carriers against the electric field (28, 29). Since this is obviously an inefficient process, recombination of charge carriers is greatly enhanced reducing the photocurrent and, hence, resulting in the typical s-shape as described above. While present due the low workfuction of the anode compared to the HOMO level of the donor (acceptor), this s-shape is, thus, not caused by an extraction barrier at the anode/donor interface itself.

Returning to our devices; the application of a positive bias results in the accumulation of negative ions at the donor/anode interface. This results in a decrease of the hole injection barrier, increasing the device current during forward bias, as is shown in the Supporting Information and is commonly seen in LECs (3). The decrease of the V_{oc} then appears counterintuitive as the built-in voltage of the device is actually increased (13, 14, 30−32). To explain this effect, we have to take into account that, while negative ions are accumulated at the donor/anode interface, uncompensated dye cations generate a positive ionic space-charge at the donor/acceptor interface. This results in an upward band bending of the donor energy levels effectively reducing the donor HOMO to the acceptor LUMO level offset, explaining the decrease in V_{oc} (see Scheme 1). Furthermore, since this HOMO−LUMO offset is reduced while at the same time the built-in voltage is increased, the V_{oc} is no longer larger than V_{bi} and the typical s-shape of the *IV* curve has disappeared.

The opposite effect occurs when the device is negatively biased; now anions accumulate at the donor−acceptor interface, increasing the HOMO−LUMO offset (and, hence, the V_{oc}), while at the same time cationic space charge at the donor/anode results in a decrease of the V_{bi}. Due to this effect, the s-shape of the *IV* curve gets more pronounced and the fill-factor and, consequently, the efficiency of the cell are reduced. The above-mentioned *J*−*V* shape effects around V_{oc} are visualized more clearly in Figure 3 by shifting the *J*−*V* curves in voltage, so the V_{oc}'s coincide. From this representation, it is clear that after forward biasing the s-shape of the *J*−*V* has disappeared whereas after negative biasing the larger difference between V_{oc} and V_{bi} results in a more pronounced s-shape. When the negative bias is decreased to values below 0.4 V, the V_{oc} is actually reduced due to the decrease in photocurrent due to the lower V_{bi}.

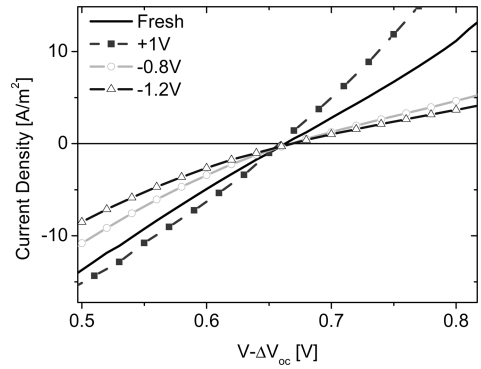

FIGURE 3. Current density to voltage characteristics of the bilayer solar cells using Cy1, compensated for the difference in V_{oc} for different prebias conditions, visualizing the shape of the *JV* around open circuit conditions.

When we now return to the devices using Cy2, we see a different behavior. Here, the built-in voltage is clearly large enough to sustain efficient charge extraction up to open circuit conditions; hole injection is efficient without the need of ion accumulation (see Supporting Information), and high fill factors of >50% are achieved. Upon biasing, we see the same behavior as in devices using Cy1: a decrease in V_{oc} upon positive biasing and an increase in V_{oc} upon negative biasing (see Figure 4). Again, the shape of the *IV*s are compared by shifting the *J*−*V* curves in voltage so the V_{oc}'s coincide (see Figure 5). When positively biased, the shape of the *J*−*V* is exactly identical to the fresh device, indicating that the V_{bi} for the fresh device is large enough to attain the maximum possible V_{oc} and a high fill factor. After negative biasing, small indications of an s-shape are appearing; however, short circuit currents are not reduced and high fill factors of >50% are maintained. Clearly, the performance of negatively biased devices surpasses the one of the fresh device, demonstrating that the presence of ions can positively affect the solar cell performance.

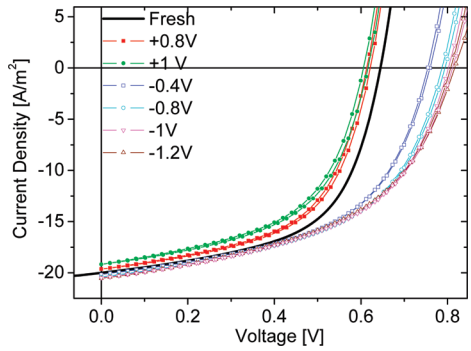

FIGURE 4. Current density to voltage characteristics of the bilayer solar cells using Cy2 under different prebias conditions. The order of poling follows the order in the legend.

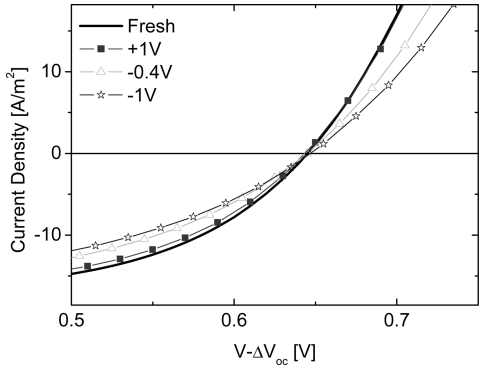

FIGURE 5. Current density to voltage characteristics of the bilayer solar cells using Cy2, compensated for the difference in V_{oc} for different prebias conditions visualizing the shape of the *JV* around open circuit conditions.

Optimization of organic solar cells is often pursued via the adjustment of the relative positions of the donor and the acceptor energy levels by molecular engineering (33, 34). The offset between the donor and acceptor LUMOs (HOMOs) provides the driving force for electron (hole) transfer but also results in a loss of energy. This loss of energy is manifested in the pristine devices employing the Cy2 dye by the relatively low open circuit voltage compared to the bandgap of the absorber. Here, we show that, using the movement of ions, it is possible to fine-tune the energy offset between donor and acceptor and increase the performance of the solar cell. This opens a new and versatile method of device optimization. The obtained results also clearly show that the accumulation of ionic space charge at the donor–acceptor interface does not hinder the generation of charge carriers, a prerequisite for the use of ionic species in photovoltaics. Even though the effects of ionic space charge presented here dissipate within 1 min (see Supporting Information), due to a reordering of the ions, the field of LECs has already shown that ions can be fixed in a number of ways, allowing for permanent changes in device performance (30, 31, 35, 36).

CONCLUSIONS

To conclude, we have shown the effects of ionic space charge on the operation of bilayer donor–acceptor solar cells. Changes in *J*–*V* characteristics can be explained by the shifting of both built-in voltage and donor–acceptor HOMO–LUMO offset. Furthermore, it is shown that the accumulation of ionic species at the charge generation interface does not hamper charge generation. In fact, it is shown that a net efficiency gain can be obtained by the redistribution of ions through poling the devices. These results allow rationalizing of future work on mixed electronic ionic systems. When a system with an ionic donor/nonionic acceptor (or vice versa) such as presented here is used, the ionic species can be used to fine-tune donor–acceptor energy level offsets (provided the built-in voltage is sufficiently large), maximizing open circuit voltages compared to LUMO–LUMO offsets. On the other hand, in a system in which both donor and acceptor support ionic conduction (and, hence, no ionic space charge is accumulated at the interface), changes in built-in voltage can be used to reduce restrictions on the used electrodes.

EXPERIMENTAL DETAILS

Prepatterned ITO-covered glass substrates are first cleaned using soapy water, demineralized water, propanol, and an UV–ozone treatment. Subsequently, a layer of PEDOT/PSS (Bayer AG) is spin-coated under ambient conditions onto the cleaned substrates, and the layer is dried by annealing the substrate for 30 min at 150 °C.

Cyanine dyes are purchased from Few Chemicals and are used without further purification. Layers of dye are spincoated from tetrafluorpropanol (2.5 mg/mL at 1000 rpm), resulting in layer thicknesses of around 40 nm as determined by profilometry. After spincoating of the dye, the substrates are transferred to a nitrogen filled glovebox (1 ppm O_2 and <1 ppm H_2O) for further processing. Here, in a first vacuum evaporator (2×10^{-6} mbar), a 40 nm layer of C_{60} (Aldrich) and 10 nm of BCP (Aldrich) is thermally evaporated. The devices are completed by thermal evaporation of a 5 nm barium/70 nm silver top contact in a separate vacuum system (2×10^{-6} mbar).

Solar cells (active area 9 mm^2) are illuminated by a white light halogen lamp in combination with interference filters for the equivalent quantum efficiency (EQE) and *J*–*V* measurement (MiniSun simulator by ECN The Netherlands) An estimation of the short-circuit current density (J_{sc}) under standard test conditions was calculated by convolving the EQE spectrum with the AM1.5G reference spectrum, using the premise of a linear dependence of J_{sc} on light intensity. *J*–*V* characteristics of the solar cells are recorded using a Keithley 2400 SourceMeter. All characterization is performed in a nitrogen filled glovebox (1 ppm O_2 and <1 ppm H_2O).

Acknowledgment. This work has been supported by the European Union FP7 program (ORION, 229036), the Spanish Ministry of Science and Innovation (MICINN; MAT2007-61584, CSD2007-00010) and the Generalitat Valenciana. The authors greatly acknowledge Alejandra Soriano and Jorge Ferrando for device preparation and testing, and technical assistance, respectively.

Supporting Information Available: Information covering CV data, IPCE curves, temporal behavior, reversability, and behavior in the dark. This material is available free of charge via the Internet at http://pubs.acs.org.

REFERENCES AND NOTES

(1) Leger, J. M. *Adv. Mater.* **2008**, *20*, 837.
(2) Inganäs, O. *Chem. Soc. Rev.* **2010**, *39*, 2633.
(3) Pei, Q.; Yu, G.; Zhang, C.; Yang, Y.; Heeger, A. J. *Science* **1995**, *269*, 1086.
(4) Pei, Q. B.; Yang, Y.; Yu, G.; Zhang, C.; Heeger, A. J. *J. Am. Chem. Soc.* **1996**, *118*, 3922.

(5) Fang, J.; Matyba, P.; Edman, L. *Adv. Funct. Mater.* **2009**, *19*, 2671.
(6) Bolink, H. J.; Coronado, E.; Costa, R. D.; Orti, E.; Sessolo, M.; Graber, S.; Doyle, K.; Neuburger, M.; Housecroft, C. E.; Constable, E. C. *Adv. Mater.* **2008**, *20*, 3910.
(7) Walzer, K.; Maennig, B.; Pfeiffer, M.; Leo, K. *Chem. Rev.* **2007**, *107*, 1233.
(8) Slinker, J. D.; Rivnay, J.; DeFranco, J. A.; Bernards, D. A.; Gorodetsky, A. A.; Parker, S. T.; Cox, M. P.; Rohl, R.; Malliaras, G. G.; Flores-Torres, F.; Abruna, H. D. *J. Appl. Phys.* **2006**, *99*, 074502.
(9) Sun, Q.; Li, Y.; Pei, Q. B. *J. Display Technol.* **2007**, *3*, 211.
(10) Wu, H.; Huang, F.; Mo, Y.; Yang, W.; Wang, D.; Peng, J.; Cao, Y. *Adv. Mater.* **2004**, *16*, 1826.
(11) Bolink, H. J.; Brine, H.; Coronado, E.; Sessolo, M. *ACS Appl. Mater. Interfaces* **2010**, *2*, 2694.
(12) Green, M. A.; Emery, K.; Hishikawa, Y.; Warta, W. *Prog. Photovoltaics* **2010**, *18*, 144.
(13) Leger, J. M.; Patel, D. G.; Rodovsky, D. B.; Bartholomew, G. P. *Adv. Funct. Mater.* **2008**, *18*, 1212.
(14) Gao, J.; Yu, G.; Heeger, A. J. *Adv. Mater.* **1998**, *10*, 692.
(15) Zhang, Y.; Hu, Y.; Gao, J. *Appl. Phys. Lett.* **2007**, *91*, 33509.
(16) Ding, L.; Jonforsen, M.; Roman, L. S.; Andersson, M. R.; Inganäs, O. *Synth. Met.* **2000**, *110*, 133.
(17) Bernards, D. A.; Flores-Torres, S.; Abruña, H. D.; Malliaras, G. G. *Science* **2006**, *313*, 1416.
(18) Benmansour, H.; Castro, F. A.; Nagel, M.; Heier, J.; Hany, R.; Nuesch, F. *Chimia* **2007**, *61*, 787.
(19) Hodgkiss, J. M.; Tu, G. L.; Albert-Seifried, S.; Huck, W. T. S.; Friend, R. H. *J. Am. Chem. Soc.* **2009**, *131*, 8913.
(20) Fan, B.; de Castro, F. A.; Chu, B. T. T.; Heier, J.; Opris, D.; Hany, R.; Nuesch, F. *J. Mater. Chem.* **2010**, *20*, 2952.
(21) Gommans, H.; Verreet, B.; Rand, B. P.; Muller, R.; Poortmans, J.; Heremans, P.; Genoe, J. *Adv. Funct. Mater.* **2008**, *18*, 3686.
(22) Fan, B.; Hany, R.; Moser, J. E.; Nuesch, F. *Org. Electron.* **2008**, *9*, 85.
(23) Fan, B.; de Castro, F. A.; Heier, J.; Hany, R.; Nuesch, F. *Org. Electron.* **2010**, *11*, 583.
(24) Brabec, C. J.; Cravino, A.; Meissner, D.; Sariciftci, N. S.; Fromherz, T.; Rispens, M. T.; Sanchez, L.; Hummelen, J. C. *Adv. Funct. Mater.* **2001**, *11*, 374.
(25) Rand, B. P.; Burk, D. P.; Forrest, S. R. *Phys. Rev. B* **2007**, *75*, 115327.
(26) Mihailetchi, V. D.; Blom, P. W. M.; Hummelen, J. C.; Rispens, M. T. *J. Appl. Phys.* **2003**, *94*, 6849.
(27) Gregg, B. A.; Hanna, M. C. *J. Appl. Phys.* **2003**, *93*, 3605.
(28) Cheyns, D.; Poortmans, J.; Heremans, P.; Deibel, C.; Verlaak, S.; Rand, B. P.; Genoe, J. *Phys. Rev. B* **2008**, *77*, 165332.
(29) Uhrich, C.; Wynands, D.; Olthof, S.; Riede, M. K.; Leo, K.; Sonntag, S.; Maennig, B.; Pfeiffer, M. *J. Appl. Phys.* **2008**, *104*, 43107.
(30) Yu, Z. B.; Sun, M. L.; Pei, Q. B. *J. Phys. Chem. B* **2009**, *113*, 8481.
(31) Leger, J. M.; Rodovsky, D. B.; Bartholomew, G. R. *Adv. Mater.* **2006**, *18*, 3130.
(32) Yang, J.; Garcia, A.; Nguyen, T.-Q. *Appl. Phys. Lett.* **2007**, *90*, 103514.
(33) Kroon, R.; Lenes, M.; Hummelen, J. C.; Blom, P. W. M.; De Boer, B. *Polym. Rev.* **2008**, *48*, 531.
(34) Scharber, M. C.; Wuhlbacher, D.; Koppe, M.; Denk, P.; Waldauf, C.; Heeger, A. J.; Brabec, C. L. *Adv. Mater.* **2006**, *18*, 789.
(35) Gao, J.; Li, Y. F.; Yu, G.; Heeger, A. J. *J. Appl. Phys.* **1999**, *86*, 4594.
(36) Hoven, C. V.; Wang, H. P.; Elbing, M.; Garner, L.; Winkelhaus, D.; Bazan, G. C. *Nat. Mater.* **2010**, *9*, 249.

AM1008216